Proceedings of the 6th JFPS International
Symposium on Fluid Power, TSUKUBA 2005
November 7-10, 2005

NUMERICAL SIMULATION OF A SLIPPER MODEL FOR WATER HYDRAULIC PUMPS/MOTORS IN MIXED LUBRICATION

Toshiharu KAZAMA

Department of Mechanical Systems Engineering
Muroran Institute of Technology
27-1, Mizumoto-cho, Muroran, 050–8585, Japan
(E-mail: kazama@mmm.muroran-it.ac.jp)

ABSTRACT

This paper presents a time-dependent mathematical model of a hybrid (hydrostatic/hydrodynamic) thrust pad bearing as a slipper of swash-plate type axial piston pumps and motors for the use of tap water under mixed and fluid film lubrication condition. Effects are examined of the load eccentricity, time-lag of changes in the supply pressure and load, surface roughness, recess volume, and the revolution radius. The bearing's motion is simulated three-dimensionally, including roughness interaction and asperity contact. Solutions are obtained regarding the friction, flow rate, power loss, and stiffness. Calculations indicate that the eccentric load causes local contacts. The preceding change in the load poses a larger motion of the bearing. The hydrodynamic effect becomes marked as the revolution radius increases. As the recess volume increases, the bearing stiffness decreases.

KEYWORDS

Water-hydraulics, Tribology, Hybrid/Hydrostatic bearings, Mixed lubrication, Piston pumps/motors

NOMENCLATURE

a : Ratio of recess radius = R_1/R_2
$\bar{H}$: Reference clearance
$\bar{h}$: Clearance = h/H
h_{0s} : Pad center clearance = h_0/σ
$\bar{I}$: Moment of inertia = $\hat{I}\ (H/R_2)^3=\omega H^3 I/(6\mu {R_2}^6)$
K : Bulk modulus of lubricant
$\bar{L}$: Power loss = $L/(\omega p_{s0} {R_2}^3 S_o)$
$\bar{M}$: Moment-load = $M/(p_{s0} {R_1}^3 S_o)$
$\bar{p}$: Pressure = $p/(p_{s0}S_o)$
$\bar{p}_r$: Recess pressure = $p_r/(p_{s0}S_o)$
$\bar{p}_s$: Supply pressure = $p_s/(p_{s0}S_o)$
$\bar{Q}$: Flow rate = $Q/(\omega {R_2}^3)$
$\bar{R}_0$: Radius of revolution = R_0/R_2
R_2 : Outer radius of bearing
$\bar{r}$, θ , $\bar{z}$: Coordinates = r/R_2, θ , z/H
$\bar{r}_w$: Eccentric ratio of load = r_w/R_2
$\bar{S}_o$: Parameter = $\hat{S}_0\ (R_2/H)^2 = 6\mu\omega(R_2/H)^2/p_{s0}$
$\bar{T}$: Friction torque = $T/(p_{s0} {R_2}^3 S_o)$
$\bar{V}_r$: Recess volume = $\hat{V}_r\ (R_2/H)^2 = 6\mu\omega V_r/(H^2 K R_2)$
$\bar{W}$: Load = $W/(p_{s0} {R_2}^2 S_o)$
X, Y, Z: Coordinates
x, y, z : Coordinates
$\bar{\alpha}$: Inclination of pad = $\alpha R_2/H$
β : Parameter of restrictor = $\hat{\beta}\ (H/R_2)^3=4H^3 l_c/(3 {r_c}^4)$
$\Delta\tau$: Time lag of load = $\Omega\Delta t$
ζ_0 : Parameter = $2W_0 \log a/[(1-a^2)p_{s0} {R_2}^2]$
μ : Viscosity
σ : Surface roughness = $({\sigma_1}^2+{\sigma_2}^2)^{1/2}$
τ : Time = Ωt
$\bar{\Phi}_{x,y}$: Angle = $\Phi_{x,y} R/H$
φ : Azimuth of pad
Ω : Reference angular velocity

Ω' : Angular velocity of sliding plane
ω : Angular velocity of pad

Subscripts:

a : Asperity
f : Fluid
m : Mean value
x, y, z : *x, y, z* axes, respectively
0 : Reference (High-pressure period)

INTRODUCTION

As a power transfer medium of hydraulic systems, nothing in nature is more human compatible and environmentally compatible than tap water: it is non-toxic, non-flammable, clean, easily disposable and readily available. In recent years, economic and environmental forces have helped water to regain its prominence as a hydraulic fluid [1][2].

Nevertheless, disadvantages and challenges of tap-water hydraulic systems remain: leakage resulting from water's low viscosity, erosion because of water's higher vapor pressure, and corrosion because of water's chemical reaction, in addition to bacterial growth and limited operating temperatures. In particular, lower viscosity and a lower viscosity-pressure index engender inferior lubrication.

As with oil-hydraulic pumps and motors, tap-water hydraulic pumps and motors are expected to function suitably in widely variant operating conditions. The efficiency and durability of the equipment are conspicuously influenced by tribological characteristics of the bearing and seal parts.

Swash-plate type axial piston pumps and motors take advantage of high power density based on high pressure and compactness, and high efficiency of variable displacement machinery. Main bearings and seal parts of the pumps and motors form a slipper, which functions as a hydrostatic bearing [3]. It is suitable for lubrication with low viscous fluids. Shute and Turnbull undertook a pioneering study [4]; later, Iboshi and Yamaguchi [3] as well as Hooke, et al. [5–6] contributed to study in this area by investigating characteristics of slippers and by discussing effects of operating conditions and geometry.

Typical hydrostatic bearings are usually designed and used under the full film lubricating condition [7–8]. However, hydraulic pumps and motors strongly demand less leakage and compactness, which enforces smaller clearance of the same order as the roughness height. The bearings of real-life pumps and motors are thus required to operate in a mixed lubrication regime.

Yamaguchi and Matsuoka developed a mixed lubrication model that is applicable to bearing and seal parts of hydraulic equipment [9]. This model is based on a combination of the asperity-contacting model proposed by Greenwood and Williamson (GW model) [10] and the average flow model by Patir and Cheng (PC model) [11–12]. The former is a model for a contact mechanism of non-lubricated stationary rough surfaces. The latter is an approach using fluid film lubrication to the contact phenomena of surface asperities. They fill the gap separating these two extreme models. Moreover, they include effects of adsorption of lubricants, elastohydrodynamic lubrication (EHL) and cavitation around asperities. Comparison of numerical results using the model and many experimental data for thrust washers and hydrostatic bearings [13–14] shows good agreement. Subsequently, Yamaguchi, et al. [15] expanded the model to include plastic-to-metal contact under water lubricated conditions, whereas the primary model specifically describes metal-to-metal contact under oil lubricated conditions.

In this study, the author applies the mixed lubrication model [9] to unsteady analysis [16] of a water-lubricated hybrid/hydrostatic thrust pad bearing, which is a model of a slipper of swash-plate type axial piston pumps and motors. Three-dimensional motion of the bearing is simulated and the tribological characteristics are discussed. Effects of interference in roughness asperities, contact between the surfaces and the time lag of the dynamic load are examined.

THEORY

Theoretical model

A hybrid thrust bearing that functions as hydrostatic and hydrodynamic bearings, lubricated with tap water, is shown in Fig. 1. Surface roughness, asperity contact, eccentric loads, and changes in the supply pressure and the load are considered. Heat generation resulting in a change in the physical properties of the lubricant and thermal distortion as well as elastic deformation of the bearing parts are neglected.

The load acting on the bearing and seal parts of hydraulic pumps and motors fundamentally changes cyclically and synchronously with the supply pressure. However, the load change can be slightly preceded or delayed because of factors such as friction and inertia of the parts in the equipment. Thus, the supply pressure p_s and the load W (<0) with a time lag $\Delta\tau$ between p_s and W are given as those in Fig. 2. Let $\Delta\tau$ be a negative value when the change in W is preceded by p_s. Revolution of the sliding plane with angular velocity Ω' as well as rotation with the angular velocity ω and reciprocation of the pad are included in the non-steady mixed lubrication modeling. The condition corresponds to a slipper of swash-plate type axial piston pumps and motors with slight inclination of the swash-plate, where the influences of pistons and ball joints are omitted.

Derivation of basic equations

The load-carrying capacity of asperities in contact is estimated by their capacities because of elastic and plastic contact. The asperity-contact pressure $\overline{p}_a$ averaged over a small apparent area, is [9, 10, 13]:

$$\left.\begin{aligned} \overline{p}_{ae} &= (2/3)\overline{E}'\left(\eta\beta'\sigma^*\right)(\sigma^*/\beta')^{1/2} \\ &\quad\times[F_{3/2}(d_e^*) - F_{3/2}(d_e^* + w_p^*)] \\ \overline{p}_{ap} &= \pi\overline{H}_a\left(\eta\beta'\sigma^*\right)F_1(d_e^* + w_p^*) \end{aligned}\right\} \quad (1)$$

Therein, d_e^* is the separation, $\bar{E}'$ ($=E'/(p_{s0}S_o)$) is the equivalent modulus of elasticity, $\bar{H}_a$ ($=H_a/(p_{s0}S_o)$) is the hardness of the softer material, $w^*_p=(\beta'/\sigma^*)(2h_a/E')^2$, β' is the radius of asperity, η is the density of asperity and σ^* ($= 0.7\,\sigma$) is the standard deviation of the asperity-summit height. Subscripts e and p respectively represent the elastic and plastic deformation of asperities. In addition, the function F_m is expressed as the following.

$$F_m(h_s)=\int_{hs}^{\infty}(s-h_s)^m\psi(s)\,ds \tag{2}$$

Therein, $\psi(s)$ is the standard probability density function, $=(2\pi)^{-1/2}\exp(-s^2/2)$. The standard plane of rough surfaces is either the summit mean plane or the surface mean plane. The former is used in the GW model and the latter in the PC model. The relation of $d_e^*=h_s$ ($h_s\geq 1.8$) and $d_e^*=1.5h_s-0.9$ ($h_s<1.8$) holds for these mean planes [17]. Following the PC model [11–12], the average Reynolds equation is described as the following.

$$\begin{aligned}&\frac{1}{\bar{r}}\frac{\partial}{\partial\bar{r}}\left(\phi\bar{h}^3\bar{r}\frac{\partial\bar{p}_f}{\partial\bar{r}}\right)+\frac{1}{\bar{r}^2}\frac{\partial}{\partial\theta}\left(\phi\bar{h}^3\frac{\partial\bar{p}_f}{\partial\theta}\right)\\&=\frac{\Omega'}{\omega}\bar{R}_0\sin\theta\left(\frac{\partial\bar{h}_T}{\partial\bar{r}}+\frac{\sigma}{H}\frac{\partial\phi_s}{\partial\bar{r}}\right)+\left(\frac{\Omega'}{\omega}+1\right)\frac{\partial\bar{h}_T}{\partial\theta}\\&+\frac{\Omega'}{\omega}\frac{\bar{R}_0}{\bar{r}}\cos\theta\left(\frac{\partial\bar{h}_T}{\partial\theta}+\frac{\sigma}{H}\frac{\partial\phi_s}{\partial\theta}\right)+\left(\frac{\Omega'}{\omega}-1\right)\frac{\sigma}{H}\frac{\partial\phi_s}{\partial\theta}+2\frac{\Omega}{\omega}\frac{\partial\bar{h}_T}{\partial\tau}\end{aligned} \tag{3}$$

Therein, ϕ and ϕ_s are the factors of surface roughness [11–12]. The boundary conditions of the fluid pressure are determined by: $\bar{p}_f(a,\ \theta,\ \tau)=\bar{p}_r(\tau)$ and $\bar{p}_f(1,\ \theta,\ \tau)=\bar{p}_e$ (atmospheric pressure). Cavitation conditions are selected such that the negative values are replaced by zero during the calculation when $\bar{p}_f<0$. Mean clearance h_T^* is shown as the following [13].

$$\begin{aligned}\bar{h}_T^*&=\bar{h}+\frac{\sigma}{H}\int_{hs}^{\infty}(s-h_s)\psi(s)ds\\&=\bar{h}_0+\bar{\alpha}\,\bar{r}\cos(\varphi-\theta)+(\sigma/H)F_1(h_s)\end{aligned} \tag{4}$$

The moment-load-carrying capacities $\bar{M}_x$ and $\bar{M}_y$ with regard to the x and y axes and the load-carrying capacity $\bar{W}$, because of contacting asperity and fluid, are computed respectively using the following integrals.

$$\bar{M}_{ax,\,fx}=\int_0^{2\pi}\int_a^1\bar{p}_{a,f}\bar{r}^2\sin\theta d\bar{r}d\theta \tag{5}$$

$$\bar{M}_{ay,\,fy}=-\int_0^{2\pi}\int_a^1\bar{p}_{a,f}\bar{r}^2\cos\theta d\bar{r}d\theta \tag{6}$$

$$\bar{W}_{a,f}=\int_0^{2\pi}\int_0^1\bar{p}_{a,f}\bar{r}d\bar{r}d\theta \tag{7}$$

The integrals of the capacities are calculated numerically with the cavitation conditions ($\bar{p}_a=0$ and $\bar{p}_f=\bar{p}_r$ in the region of $\bar{r}<a$).
Considering the fluid compressibility and displacement volume in the recess, the recess pressure $\bar{p}_r$ satisfies the following relation.

$$\bar{V}_r\frac{\Omega}{\omega}\frac{d\bar{p}_r}{d\tau}=\bar{Q}_r-\bar{Q}(a)-\pi a^2\frac{\Omega H}{\omega R_2}\frac{d\bar{h}_0}{d\tau} \tag{8}$$

Therein, $\bar{Q}_r$ and $\bar{Q}(\bar{r})$ ($a\leq\bar{r}\leq 1$) are the flow rates though the capillary restrictor and the bearing-land, given respectively as the following.

$$\bar{Q}_r=\pi(H/R_2)(\bar{p}_s-\bar{p}_r)/\beta \tag{9}$$

$$\bar{Q}(\bar{r})=\frac{H}{R_2}\frac{\bar{r}}{2}\int_0^{2\pi}\left[\begin{aligned}&-\phi\bar{h}^3\frac{\partial\bar{p}_f}{\partial\bar{r}}\\&+\frac{\Omega'}{\omega}\bar{R}_0\sin\theta\left(\bar{h}_T^*+\frac{\sigma}{H}\phi_s\right)\end{aligned}\right]d\theta \tag{10}$$

The equations describing the bearing-pad motion are thus written as the following.

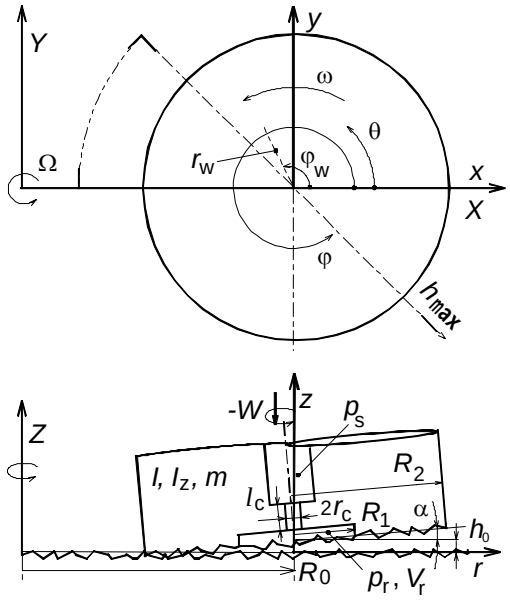

Fig. 1 Schematic diagrams and coordinates of the slipper model (hybrid thrust pad bearings)

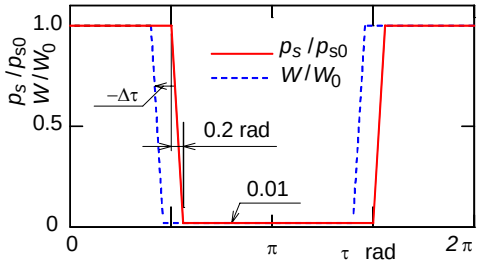

Fig. 2 Changes in supply pressure p_s and load W with a time lag $\Delta\tau$

$$\bar{m}\frac{d^2\bar{h}_0}{d\tau^2} = \bar{W}_a + \bar{W}_f + \bar{W} - \bar{g}\,\bar{m} \tag{11}$$

$$\bar{I}_x\frac{d^2\bar{\Phi}_x}{d\tau^2} - \bar{I}_z\frac{\omega}{\Omega}\frac{d\bar{\Phi}_y}{d\tau} = -\bar{M}_{ax} - \bar{M}_{fx} - \bar{M}_x \tag{12}$$

$$\bar{I}_y\frac{d^2\bar{\Phi}_y}{d\tau^2} + \bar{I}_z\frac{\omega}{\Omega}\frac{d\bar{\Phi}_x}{d\tau} = \bar{M}_{ay} + \bar{M}_{fy} + \bar{M}_y \tag{13}$$

In those equations, $\bar{g}=g/(\Omega^2 H)$, $\bar{I}_x$, $\bar{I}_y$ and $\bar{I}_z$ represent the respective moment of inertia for the x, y and z axes, $\bar{\Phi}_x = -\bar{\alpha}\sin\varphi$ and $\bar{\Phi}_x = -\bar{\alpha}\cos\varphi$.
Furthermore, the friction torque $\bar{T}_a$, because of the asperities in contact, and the torque $\bar{T}_f$, because of fluid acting on the sliding surface, are formulated as below.

$$\bar{T}_f = \frac{H}{6R_2}\int_0^{2\pi}\int_a^1 \left\{\begin{array}{l}\dfrac{\bar{r}^3}{\bar{h}}\left[1-\dfrac{\Omega'}{\omega}\left(\dfrac{\bar{R}_0}{\bar{r}}\cos\theta+1\right)\right] \\ \left[\phi_f + \left(1-2\dfrac{\sigma_1^{\,2}}{\sigma^2}\right)\phi_{fs}\right] - 3\phi_{fp}\bar{h}\bar{r}\dfrac{\partial\bar{p}_f}{\partial\theta}\end{array}\right\} d\bar{r}d\theta \tag{14}$$

$$\bar{T}_a = \iint_{\bar{A}_0}\bar{r}\left[\xi\bar{\tau}_p\left(\frac{\bar{\tau}_e}{\bar{\tau}_p}d\bar{A}_e + d\bar{A}_p\right) + (1-\xi)\bar{\tau}_{ad}d\bar{A}_r\right] \tag{15}$$

Therein, $\bar{A}_0$ ($=A_0/R_2^2$) is the land area, $\bar{A}_r$ is the real contacting area, $d\bar{A}$ ($=\bar{r}d\bar{r}d\theta$) is the apparent area, ξ is the parameter regarding an area-ratio of solid-contact asperities [9], $\bar{\tau}$ ($=\tau/[6\mu\omega(R_2/H)^2]$) is the shearing strength, $\bar{\tau}_{ad}$ is shearing strength of the adsorbed film, and both ϕ_f and ϕ_{fs} are factors of roughness [11–12].
Defining the mean power loss $\bar{L}_m$ during a single cyclic period by summing and averaging the power losses because of leakage flow rate $\bar{L}_{Qm}$ and friction torque $\bar{L}_{Tm}$ yields the following relationship.

$$\bar{L}_m = \frac{1}{2\pi}\int_0^{2\pi}\left[\bar{p}_s\bar{Q}_{out} + \bar{T}_a + \bar{T}_f\right]d\tau = \bar{L}_{Qm} + \bar{L}_{Tm} \tag{16}$$

The reference operating condition is representable as the ratio ζ_0 of the hydrostatic balance in the high-pressure period in a steady state defined by the following.

$$\zeta_0 = 2W_0\log a/\left[\pi\left(1-a^2\right)p_{s0}R_2^2\right] \tag{17}$$

Therein, W_0 is the load (<0). The dynamic stiffness and moment-stiffness are defined as below.

$$\lambda = \left|\bar{W}_{\max} - \bar{W}_{\min}\right| / \left|\bar{h}_{0\max} - \bar{h}_{0\min}\right| \tag{18}$$

$$\lambda_M = \left|\bar{M}_{\max} - \bar{M}_{\min}\right| / \left|\bar{\alpha}_{\max} - \bar{\alpha}_{\min}\right| \tag{19}$$

Numerical technique

The Runge-Kutta method is used in solving the set of equations described in the previous section. The effects of cavitation and the inertia terms in the equations of motion are included in the following calculation [3].
The representative numerical parameters are specified as: the ratio a of the recess radius is 0.683, the moment of inertia $\hat{I}$ for the x and y axes is 9.3×10^5, the moment of inertia $\hat{I}_z$ for the z axis is 4.7×10^5, bearing-mass $\hat{m}$ is 9.3×10^5, the revolution radius $\bar{R}_0$ is three, the outer bearing-radius R_2 is 10 mm, the load-eccentric ratio $\bar{r}_w$ is 0.1, the operating parameter $\hat{S}_0$ is 2×10^{-7}, the recess volume $\hat{V}_r$ is 1×10^{-10}, restrictor parameter $\hat{\beta}$ is 5.7×10^{10}, the parameter ζ_o [13] is two-thirds, surface roughness σ/R_2 is 2×10^{-4}, roughness-ratio σ_2/σ_1 is unity, azimuth φ_w of the load is $\pi/2$, and the ratio of angular velocity Ω/ω is unity. The parameters regarding mixed lubrication are given by Ref. [15].

RESULTS AND DISCUSSION

Effects of load eccentricity

Figures 3 and 4 demonstrate the time evolution of the center clearance h_{0s}, pad inclination $\bar{\alpha}$ and the pad azimuth φ as well as the maximum contact pressure $\bar{p}_{a\max}$ and the leakage flow rate $\bar{Q}_{out}$ [$=\bar{Q}_r(\bar{r}=1)$] in terms of eccentric ratio $\bar{r}_w$ of the load, where the changes in $\bar{p}_s$ and $\bar{W}$ are synchronized ($\Delta\tau$=0).
As the ratio $\bar{r}_w$ increases, the parameters h_{0s}, $\bar{\alpha}$ and φ become large in the low-pressure period and the pressure $\bar{p}_{a\max}$ increases in the high-pressure period. The leakage $\bar{Q}_{out}$ peaks at the transition from the low-pressure to the high-pressure period, which is caused by the squeeze film effect.

Effect of time lag of loads

Figures 5–7 depict the variation of the center

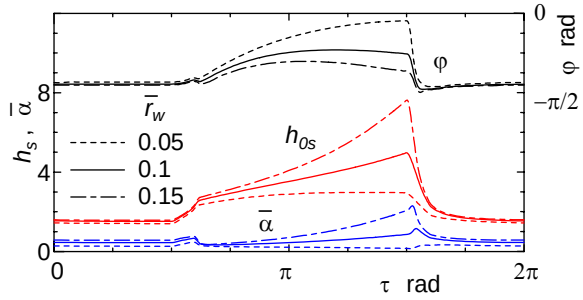

Fig. 3 Changes in center clearance h_{0s}, inclination $\bar{\alpha}$ and azimuth φ of pad in terms of eccentric ratio $\bar{r}_w$ of load ($\Delta\tau$=0)

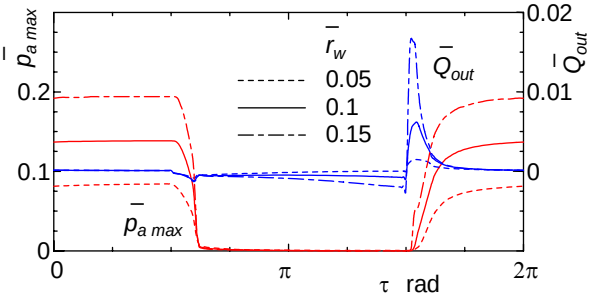

Fig. 4 Changes in maximum contact pressure $\bar{p}_{a\max}$ and leakage flow rate $\bar{Q}_{out}$ in terms of eccentric ratio $\bar{r}_w$ of load ($\Delta\tau$=0)

clearance h_{0s} and minimum clearance $h_{min\,s}$, leakage flow rate $\overline{Q}_{out}$, total friction torque $\overline{T}$ ($\overline{T}_a + \overline{T}_f$) and the ratios of cavitation area $\overline{A}_{cav}/\overline{A}_0$ and contact area $\overline{A}_{cnt}/\overline{A}_0$ with time lag $\Delta\tau$ conditions. When the change in the load precedes that in the supply pressure ($\Delta\tau<0$), the hydrostatic load-carrying capacity momentarily exceeds the load at $\tau\approx\pi/2$, which causes an imbalance and larger clearances in the low-pressure period. Jumping of the pad yields cavitation in the bearing-land; thereby creating the peaks of $\overline{A}_{cav}/\overline{A}_0$. At another transition of the pressure and the load ($\tau\approx3\pi/2$), the downward force becomes larger than that which is exerted upward, which consequently increases leakage $\overline{Q}_{out}$ based on the squeeze film effect.

Conversely, when the change in the load delays ($\Delta\tau>0$) at $\tau\approx\pi/2$, the downward force becomes larger and the pad is suppressed *vice versa*.

During the high-pressure period, the surfaces remain in contact ($\overline{A}_{cnt}/\overline{A}_0=1$) resulting in larger torque $\overline{T}$ because of asperity-contact. On the other hand, during the low-pressure period, the area ratio $\overline{A}_{cnt}/\overline{A}_0$ is less than unity or equal to zero and $\overline{Q}_{out}$ and $\overline{T}$ are infinitesimal.

Effect of radius of revolution of pad

The radius $\overline{R}_0$ of the revolution of the pad corresponds to the respective pitch radius of the cylinder-bores of piston pumps and motors. Figures 8 and 9 show the effect of $\overline{R}_0$ on the bearing. As $\overline{R}_0$ increases, the maximum $\overline{h}_{0\max}$ of the center clearance increases, especially in the low-pressure periods, because of the hydrodynamic (wedge) effect; the minimum $\overline{h}_{0\min}$ changes less. The increase in hydrodynamic load-carrying capacity lessens the cavitation period $\tau_{cav}/2\pi$ and contacting period $\tau_{cnt}/2\pi$ in a cycle.

Effect of recess volume or liquid bulk modulus

The effect of the normalized recess volume $\overline{V}_r$ on pad fluctuation is examined in Fig. 10. As $\overline{V}_r$ increases, the bearing-stiffness $\overline{\lambda}$ decreases. By contrast, the moment stiffness $\overline{\lambda}_M$ remains almost constant. The mean power loss $\overline{L}_m$ is determined by the power loss $\overline{L}_{Tm}$ because of friction torque and the losses decrease slightly with increased $\overline{V}_r$.

It is noteworthy that parameter $\hat{V}_r$ is equivalent to the inverse number of the bulk modulus K of the liquid. Therefore, if K is reduced, *e.g.* by containing bubbles in the liquid, the pad would fluctuate distinctly and the bearing-stiffness would decrease.

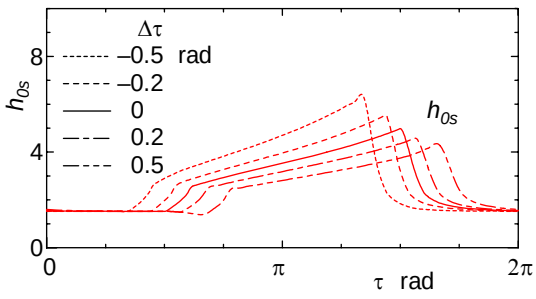

Fig. 5 Changes in center clearance h_{s0} in terms of time lag $\Delta\tau$ of the load

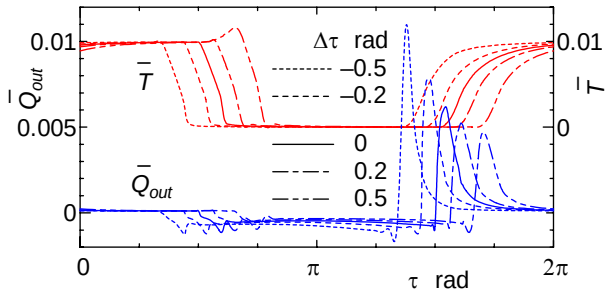

Fig. 6 Changes in leakage flow rate $\overline{Q}_{out}$ and friction torque $\overline{T}$ in terms of time lag $\Delta\tau$ of the load

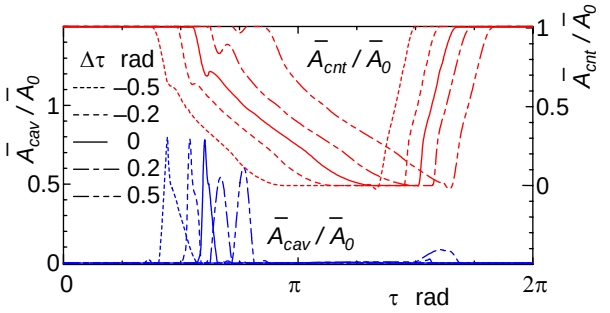

Fig. 7 Changes in cavitation area $\overline{A}_{cav}/\overline{A}_0$ and contact area $\overline{A}_{cnt}/\overline{A}_0$ in terms of time lag $\Delta\tau$ of the load

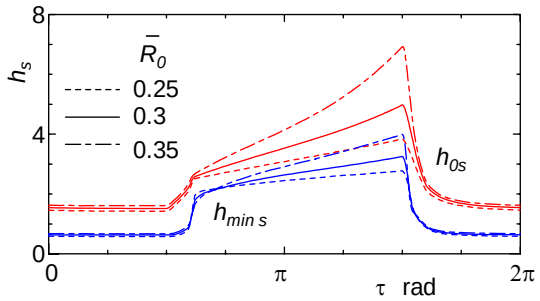

Fig. 8 Changes in center h_{s0} and minimum $h_{s\,min}$ clearances in terms of revolution radius $\overline{R}_0$

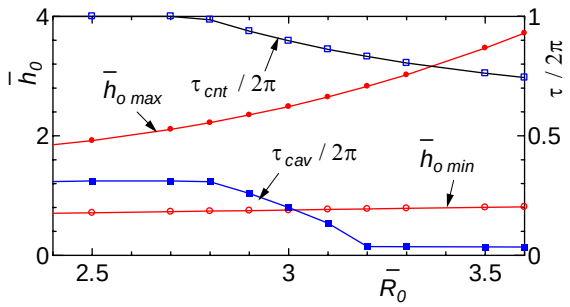

Fig. 9 Effect of revolution radius $\overline{R}_0$ on maximum clearance $\overline{h}_{0\max}$, minimum clearance $\overline{h}_{0\min}$, cavitation period $\tau_{cav}/2\pi$ and contacting period $\tau_{cnt}/2\pi$

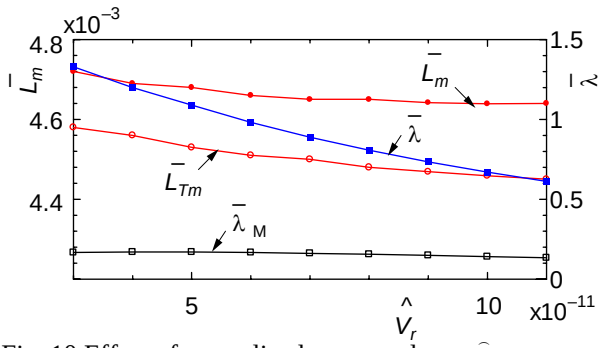

Fig. 10 Effect of normalized recess volume $\hat{V}_r$ on mean power loss $\bar{L}_m$, mean friction power loss $\bar{L}_{Tm}$, dynamic stiffness $\bar{\lambda}$, and moment-stiffness $\bar{\lambda}_M$

CONCLUDING REMARKS

A hybrid thrust bearing as a slipper model of water hydraulic piston pumps and motors was developed in this study. It includes uneven contact because of alignment in mixed and fluid film lubrication, based on the GW model and the PC model. Numerical solutions of the time-dependence problem are obtained over a wide range of operation under water lubricated conditions.

The following conclusions were obtained: i) As the eccentric ratio of the load increases, the inclination of the pad increases, thereby causing local asperity-contact pressure. ii) The time lag between the supply pressure and the load influences the bearings' motion and tribological characteristics. In particular, the preceding change in loads engenders a larger motion of the pad. iii) The radius of revolution of the pad influences the bearing performance because of hydrodynamic wedge effect. iv) As the recess volume increases or the bulk modulus decreases, the bearing motion is enlarged, especially in the low-pressure period, decreasing the bearing stiffness.

ACKNOWLEDGEMENTS

The author would like to thank Professor Emeritus Atsushi Yamaguchi of Yokohama National University and Emeritus Professor Mitsuru Fujiwara of Muroran Institute of Technology for their thoughtful encouragement.

REFERENCES

1. Yamaguchi, A., Tap Water – Possibility as a Hydraulic Fluid, Journal of Japan Hydraulic and Pneumatic Society, 1978, 9–4, pp. 205–210. (in Japanese)
2. Modern Water Hydraulics – Our Choice for the Future, 1995, National Fluid Power Association.
3. Iboshi, N. and Yamaguchi, A., Characteristics of a Slipper Bearing for Swash Plate Type Axial Piston Pumps and Motors (1st Report), Bulletin of Japan Society of Mechanical Engineers, 1982, 25, pp. 1921–1930; (2nd Report), *ibid.*, 1983, 26, pp. 1583–1589; (4th Report), *ibid.*, 1986, 29, pp. 2539–2546.
4. Shute, N.A. and Turnbull, D.E., Minimum Power Loss of Hydrostatic Slipper Bearings for Axial Piston Machines, Proceedings of International Convention on Lubrication and Wear, Institution of Mechanical Engineers, 1963, pp. 3–14.
5. Hooke, C.J. and Kakoullis, Y.P., Effects of Non-Flatness on the Performance of Slippers in Axial Piston Pumps, Proceedings of Institution of Mechanical Engineers, Part C, 1983, 197, pp.239–247.
6. Hooke, C.J. and Li, K.Y., The Lubrication of Overclamped Slippers in Axial Piston Pumps--Centrally Loaded Behaviour, Proceedings of Institution of Mechanical Engineers, Part C, 1988, 202, pp. 287–293.
7. Williams, J.A., Engineering Tribology, 1996, Oxford Science Publications.
8. Hamrock, B.J., Fundamentals of Fluid Film Lubrication, 1994, McGraw-Hill.
9. Yamaguchi, A. and Matsuoka, H., A Mixed Lubrication Model Applicable to Bearing and Seal Parts of Hydraulic Equipment, Journal of Tribology, Transactions of ASME, 1992, 114, pp. 116–121.
10. Greenwood, J.A. and Williamson, J.B.P., Contact of Nominally Flat Surfaces, Proceedings of Royal Society, London, Series A, 1966, 295, pp. 300–319.
11. Patir, N. and Cheng, H.S., An Average Flow Model for Determining Effects of Three-Dimensional Roughness on Partial Hydrodynamic Lubrication, Journal of Lubrication Technology, Transactions of ASME, 1978, 100, pp. 12–17.
12. Patir, N. and Cheng, H.S., Application of Average Flow Model to Lubrication Between Rough Sliding Surfaces, Journal of Lubrication Technology, Transactions of ASME, 1979, 101, pp. 220–230.
13. Kazama, T. and Yamaguchi, A., Application of A Mixed Lubrication Model for Hydrostatic Thrust Bearings of Hydraulic Equipment, Journal of Tribology, Transactions of ASME, 1993, 115, pp. 686–691.
14. Kazama, T. and Yamaguchi, A., Experiment on Mixed Lubrication of Hydrostatic Thrust Bearings for Hydraulic Equipment, Journal of Tribology, Transactions of ASME, 1995, 117, pp. 399–402.
15. Yamaguchi, A., Okamoto, Y. and Wang, X., Friction Characteristics of PEEK for Bearing and seal Parts of Water Hydraulic Equipment, Transactions of Japan Fluid Power System Society, 2003, 34-2, pp. 40–45. (in Japanese)
16. Kazama, T., Yamaguchi, A. and Fujiwara, M., Motion of Eccentrically and Dynamically Loaded Hydrostatic Thrust Bearings in Mixed Lubrication, Proceedings of 5th JHPS International Symposium on Fluid Power, 2002, pp. 233–238.
17. Johnson, K.L., Greenwood, J.A. and Poon, S.Y., Simple Theory of Asperity Contact in Elastohydrodynamic Lubrication, Wear, 1972, 19, pp. 91–108.